Full-scale testing apparatus for investigating the in situ behaviour of peat under cyclic loading

Jiarui Zhang [1*], *Tom* de Gast [2], *Cor* Zwanenburg[1,3], and *Kenneth* G. Gavin [1]

[1] Department of Geoscience and Engineering, Delft University of Technology, Delft, The Netherlands
[2] Waterschap Hollandse Delta, Ridderkerk, the Netherlands.
[3] Deltares, Delft, the Netherlands

Abstract. A considerable portion of the subsoil strata beneath railway embankments in the Netherlands contains peat layers. Consequently, knowledge is required about the behaviour of peat under cyclic loading at train passage frequencies. Due to its fibrous nature and high water content, the mechanical behaviour of peat exhibits pronounced scale effects when characterized at different scales. This paper presents the design and implementation of a full-scale cyclic loading test setup for a circular footing on peat. By using an actuator and a reaction frame to drive the circular foundation, a large number of vertical loading cycles can be applied at a loading frequency of 1 Hz. Preliminary results from the test are also presented. The test is intended to investigate the in situ response of peat under cyclic loading. These test results help bridge the gap between advanced laboratory cyclic loading tests and field-scale railway embankment boundary conditions.

1 Introduction

Peat presents considerable difficulties in the characterization of its undrained shear strength, which in turn directly affects the assessment of the bearing capacity of foundations resting on peat. In laboratory undrained tests, peat often exhibits apparently high friction angles and pore pressure ratios, without showing a clearly defined failure [1–3]. In centrifuge and other model tests, reconstituted peat generally requires a gradual increase in acceleration to avoid early failure, unless in situ samples can be obtained using specially designed large block samplers [4, 5]. Field investigation methods, such as probing tests and vane tests, are also affected by the low resistance of peat, potentially partially drained conditions, and the non-uniform distribution of fibres [6]. This also hinders the determination of its undrained shear strength. Therefore, the characterization of peat strength requires an integrated interpretation of different testing methods and the establishment of correlations among them. In this context, full-scale field testing becomes particularly important for a more accurate description of peat strength.

Similar difficulties arise in the investigation of peat behaviour under cyclic loading. When the results of cyclic undrained triaxial tests are applied to boundary value problems, such as the settlement of peat layers underneath embankments, discrepancies in drainage conditions and fibre-induced heterogeneity between laboratory and field conditions introduce unavoidable uncertainties [7, 8]. Empirical formulas or constitutive models derived from laboratory tests inevitably involve inherent limitations, and controllable full-scale field cyclic loading tests are required for comparison and validation[9].

At present, full-scale field failure tests on peat are mainly limited to static loading. Field testing under cyclic loading is considerably more difficult, primarily because sufficiently large cyclic loads must be generated at the relatively low loading frequencies relevant to train loading in the subsoil. Under the constraint of maintaining equipment safety, it is difficult to apply controllable cyclic loading to an embankment up to failure. The circular footing provides a more practical alternative. As a classical bearing-capacity problem, its failure causes less disturbance than embankment failure and is easier to restore after testing. It can also be related more directly to classical bearing-capacity theory and requires fewer assumptions in back-analysis, such as the specification of backfill parameters [10, 11]. Although the circular footing does not reproduce the full geometry of railway embankment, it provides a full-scale boundary value problem from which key in situ cyclic response characteristics and design parameters of the peat can be identified. These can then be used to calibrate laboratory-based constitutive relationships and subsequently applied in the analysis of peat layers underneath embankments.

For this reason, a field cyclic loading system was designed in the present study. This system allows vertical cyclic loads with different amplitudes to be applied to a circular footing, while settlement and pore pressure are monitored during loading. This paper presents the configuration of the loading system and selected test results.

* Corresponding author: J.Zhang-20@tudelft.nl

2 Geotechnical Conditions

The test was carried out at the experimental farm in Zegveld, which is representative of the peat meadow landscape of the western Netherlands. The site location is shown in Fig. 1. A substantial amount of previous field investigation and laboratory characterisation is available for this site [1, 12–14]. Borehole records indicate that the soil profile in Zegveld consists predominantly of eutrophic wood-sedge peat, overlain by an approximately 0.3 m thick layer of organic clay. This is underlain by wood peat extending to a depth of about 3 m, followed by mainly sedge and reed peat down to 6.5 m [12]. Pleistocene sand is encountered below this depth. The groundwater table is approximately 0.25 m below the ground surface.

Fig 1. Location of Zegveld test site, from [12].

Previous laboratory characterisation showed that the peat has a unit weight of 9.90 kN/m³ with a coefficient of variation (CoV) of 0.04. The water content is 592% (CoV = 0.13), and the loss on ignition (LOI) is 75% (CoV = 0.08). The preconsolidation pressure of the peat layer is approximately 9.0-15.4 kPa. Based on the peat classification system proposed by Hobbs, the peat at the site is classified as $H_{5–6}B_3F_{1–2}R_2W_2N_3TV_0TH_1$[13, 14].

3 System Design Specifications

The loading system was designed to reproduce and extend the in-situ response of peat foundations under train-induced cyclic loading. Accordingly, the cyclic load applied to the circular loading plate should, in terms of loading frequency, be as close as possible to the dominant frequency of the cyclic loading experienced by the subsoil directly beneath the track. In terms of load amplitude, it should exceed the actual train-induced load and approach the static bearing capacity of the footing, so that the response of peat under higher cyclic stress levels can be investigated.

With regard to loading frequency, the high-frequency components of the load spectrum generated by train passage attenuate rapidly with depth [15]. At subsoil level, the dominant frequency is usually governed by the spacing between adjacent bogies or by the spacing between the bogie groups located at the two ends of a carriage [16, 17]. The cyclic loading induced in the subsoil by train passage can therefore generally be approximated as a sinusoidal load with a period corresponding to this characteristic spacing. As shown in Fig. 2, taking an Intercity train type as an example, the dominant frequencies associated with the spacing between adjacent bogie groups (L_1), the spacing between bogies (L_2), and the spacing between wheelsets (L_3) at different train speeds are summarised in Table 1. For train speeds in the range of 50-150 km/h, the frequency range of interest is 0.50-5.21 Hz. In the present study, the case corresponding to L1 at a train speed of 100 km/h was adopted, resulting in a loading frequency of 1 Hz.

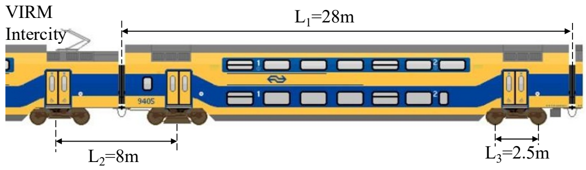

Fig 2. Schematic of Intercity train carriage dimensions.

Table 1. Dominant frequencies of an Intercity train at different speeds.

Train speed [km/h]	Frequency [Hz]		
	L1	L2	L3
50	0.50	1.74	5.55
100	0.99	3.47	11.10
150	1.49	5.21	16.65

Previous statistical analyses and finite element studies have shown that, beneath an embankment with a thin 1m sand layer, the cyclic load amplitude generated by the double decker intercity train (axle load = 22.5ton) on the top of the peat layer is approximately 13 kPa [18, 19]. This level of cyclic loading can reasonably represent the stress condition induced by train passage. However, to investigate the response of peat under cyclic loading conditions approaching instability or failure, the applied cyclic load amplitude in the test must be significantly higher than the actual train-induced loading. The results presented in Section 5.3 show that when the cyclic load amplitude was increased to 53 kPa, clear soil failure occurred.

It is not straightforward to generate cyclic loads of this magnitude at frequencies below 5 Hz in the field. Most existing full-scale field apparatus for simulating train-induced cyclic loading rely on rotating eccentric masses to generate cyclic forces through centrifugal action (e.g. Fig. 3a). Owing to rotational speed limitations, such apparatuses generally find it difficult to generate sufficient cyclic loading at frequencies lower than 10 Hz. By contrast, indoor full-scale model tests typically employ linear actuators combined with stable reaction frames and control systems to achieve cyclic loading with different amplitudes and frequencies, as shown in Fig. 3(b). To realise a comparable actuator-based system in the field, several requirements must be satisfied simultaneously, including a reliable reaction frame that can be transported and assembled easily, a stable power supply and control system, and a loading plate that is able to tilt freely and fail naturally under cyclic loading. The loading system presented in this paper was designed based on these requirements.

(a)

(b)

Fig 3. (a) Field excitation equipment, from [20] (b) indoor model test facility, from [21].

4 Test setup

As shown in Fig. 4, loading is provided by an actuator system connected to the reaction frame through a fixed hinge. The reaction frame comprised two parallel main HEB300 beams, each assembled from three 2.3 m beam segments using preloaded bolted connections, giving a total length of 6.9 m. Concrete slabs were placed on the frame to provide counterweight. The self-weight of the frame together with the counterweight load is distributed through side support beams to timber dragline mats supported at the four corners.

Fig 4. Photograph of the loading frame.

At its lower end, the actuator was connected to the loading plate by means of a spherical hinge. This arrangement allowed the loading plate to rotate freely during loading, so that failure could develop naturally. It also created a double-hinged configuration for the actuator itself, allowing it to remain vertical under self-weight and thereby reducing the risk of damage to the actuator rod caused by bending. As shown in Fig. 5, the settlement of the circular loading plate was measured by the position feedback rods located on both sides of the actuator, while the applied load was obtained from the load cell integrated into the actuator rod. The actuator was powered by a hydraulic power pack. A dedicated cooling system and battery pack were provided to ensure a stable load output over tests of up to 15,000 cycles.

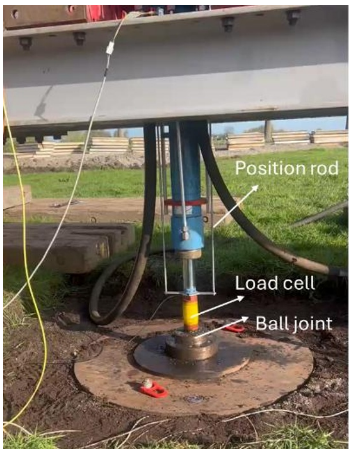

Fig 5. Configuration of the actuator system.

Table 2. Summary of the reported NPL tests and applied CSR values.

Test ID	Preloading condition	Test type	Applied CSR	Number of cycles
NPL ST-1	NPL	Static	-	-
NPL CT-1	NPL	Cyclic	0.20	15,000
NPL CT-2	NPL	Cyclic	0.39	15,000
NPL CT-3	NPL	Cyclic	0.60	15,000
NPL CT-4	NPL	Cyclic	0.78	5,200

A total of 11 tests were carried out. For each test, an excavation of approximately 2 × 2 m and about 0.3 m in depth was made to remove the surface grass roots and organic clay, thereby fully exposing the underlying peat. Six tests were preloaded (PL) with concrete slabs for four months, including two static tests (ST) and four cyclic tests (CT). The remaining five tests were conducted without preloading (NPL), including one static test and four cyclic tests. The preloading stage was intended to represent field precompression and to examine whether an increased over consolidation level modifies the bearing capacity, settlement accumulation and pore-pressure response under subsequent cyclic loading. For clarity, Table 2 summarises the test conditions of the non-preloaded (NPL) tests reported in this paper. Although the full test programme also included preloaded (PL) tests, only the preliminary results of the NPL series are presented here. The field test site overview is shown in Fig. 6.

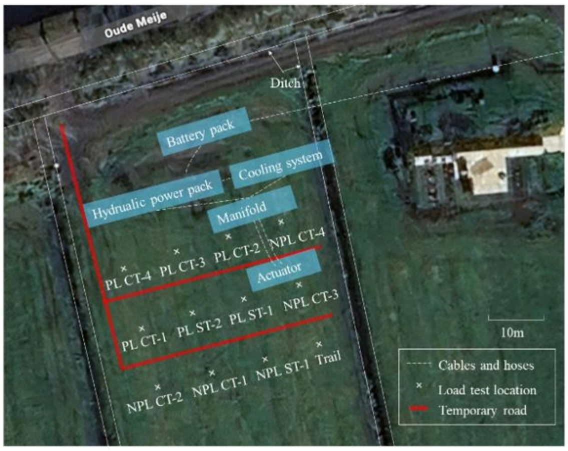

Fig 6. Test site overview.

Pore pressure transducers (PPT) were installed beneath the centre of the footing at depths of 0.5 m, 1.0 m, and 1.5 m. Total pressure transducers (TST) were installed at depths of 0.5 m and 1.0 m beneath the centre, and an additional transducer was installed at a depth of 0.8 m at a horizontal distance of 2 m from the plate edge. The instrumentation arrangement is shown in Fig. 7.

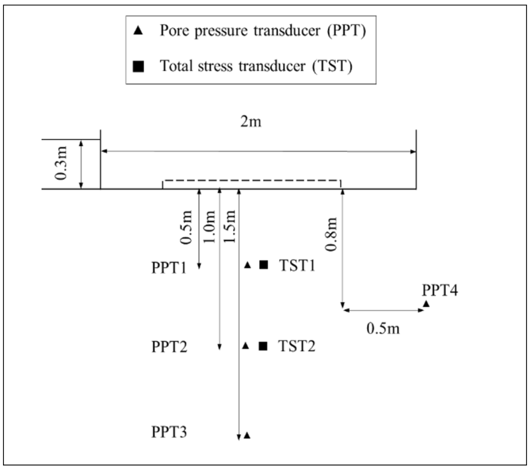

Fig 7. Section details of instrumentation.

5 Test results

5.1 In situ CPT tests

Cone penetration tests (CPTs) were carried out at the locations of both the static and cyclic loading tests, and the results for the net cone resistance, q_{net}, are shown in Fig. 8(a). q_{net} was calculated as follows according to Equation (1) [22]:

$$q_{net} = q_c + (1-a)u_2 - \sigma_{v0} \tag{1}$$

in which qc represents the uncorrected cone resistance, a is the cone area ratio (0.75 in this study), u2 is the pore pressure measured above the cone shoulder, and σv0 is the overburden pressure.

The q_{net} values mainly range from 0.1 to 0.2 MPa until the sand layer is reached at approximately -8.8 m NAP. Occasional peaks between -3 and -5 m NAP may reflect the presence of incompletely decomposed wood fragments. Fig. 8(b) shows the results for the friction ratio, R_f. Between -3 and -5 m NAP, NPL ST-1 reaches nearly 20%, while the other profiles fluctuate around 10%. With increasing depth, all R_f values decrease to around 7%. The variation in R_f may correspond to the transition from wood peat to sedge and reed peat indicated by the borehole records.

Fig. 8(c) shows the variation of u_2 and the hydrostatic pressure line with depth. The value of u_2 increases with depth but is generally lower than the hydrostatic pressure. This phenomenon might be attributed to the lateral displacement of the soil combined with tensioning of the horizontal fibres during penetration. The local expansion of pore volume during penetration leads to the generation of negative pore pressure. The CPT results at the five test locations show broadly consistent trends. The relative difference in the median q_{net} values of the five CPTs between -3 and -9 m remains within 30%, indicating that the results of the static and cyclic loading tests are comparable.

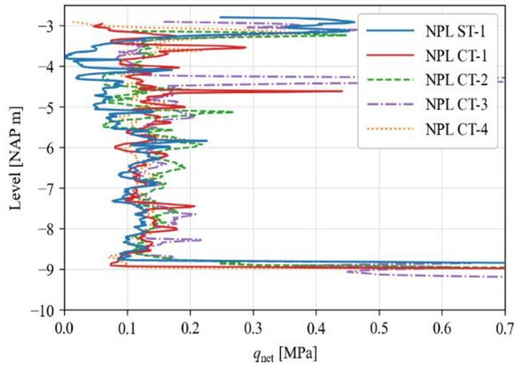

(a)

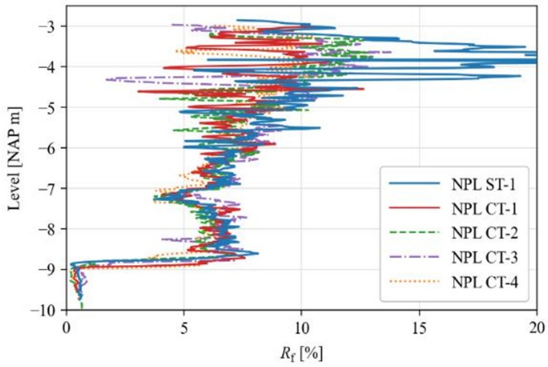

(b)

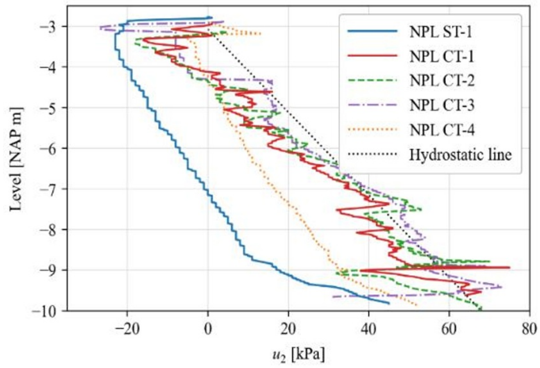

(c)

Fig 8. CPT profiles for test locations without preloading: (a) corrected cone resistance q_{net}, (b) friction ratio, R_f, and (c) pore pressure measured at the shoulder of the cone, u_2.

5.2 Static loading test

Load was applied to the circular loading plate in increments until failure to determine its bearing capacity. The load was increased by 5 kPa at each stage over a period of 1 min and then maintained at that level for 2 min. The results of the static loading test at the non-preloaded location, NPL ST-1, are presented in Fig. 9, which shows the relationship between the measured applied stress, q_{app}, and the average settlement, s_{av}, obtained from the two position feedback rods.

The settlement increased approximately linearly under the equally spaced load increments, while the creep observed during each holding stage gradually became more pronounced. When the load was increased beyond 60 kPa, it rose abruptly to approximately 78 kPa, after which a clear plastic plateau developed. The load then remained at about 68 kPa while settlement continued to increase. It can therefore be inferred that the bearing capacity of the circular loading plate, q_f, was approximately 68 kPa.

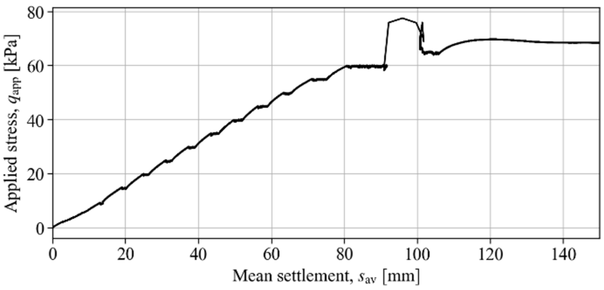

Fig 9. Settlement of the loading plate with increased stress in test NPL ST-1.

The variations in total stress, Δσ, and pore pressure, Δ*u* beneath the loading plate during the stepwise increase in load are shown in Fig. 10 as a function of time. Both the total stress and the excess pore pressure increased with each load increment. At a depth of 0.5 m, TST1 and PPT1 showed the most rapid increase, reaching approximately 19 kPa and 16 kPa before failure. With increasing depth, the development of TST2 and PPT2 at 1.0 m was significantly smaller, remaining at around 9 kPa before failure, while PPT3 at 1.5 m remained at approximately 7 kPa. The continued increase in pore pressure and total stress observed after failure was caused by further compression of the soil due to the accelerated settlement of the loading plate.

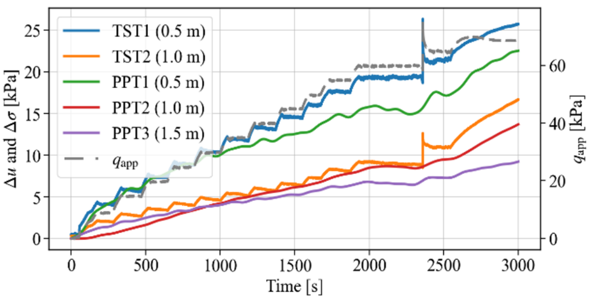

Fig 10. Applied stress, total stress change, and excess pore pressure versus time.

5.3 Cyclic loading tests

Fig. 11 shows ten representative cycles of the loading waveform for the four NPL cyclic loading tests. The cyclic load amplitude was defined as different proportions of the static bearing capacity, q_f. The cyclic stress ratio, CSR, can be defined as follows:

$$\mathrm{CSR}=\frac{q_{cyc}}{q_f} \tag{2}$$

where q_{cyc} is the amplitude of the cyclic load and q_f is the bearing capacity obtained from the static loading test. To prevent the actuator from operating under unloaded conditions, a static load component of 5.0 kPa was applied, with an actual output ranging from 5.6 to 7.2 kPa. As this component was small in comparison with the cyclic load, it was treated in this study as part of the cyclic loading. On this basis, the CSR values of the four tests were 0.20, 0.39, 0.60, and 0.78.

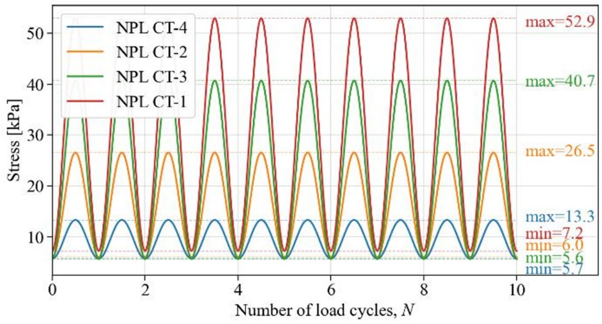

Fig 11. Schematic of the applied cyclic loading in different cyclic tests.

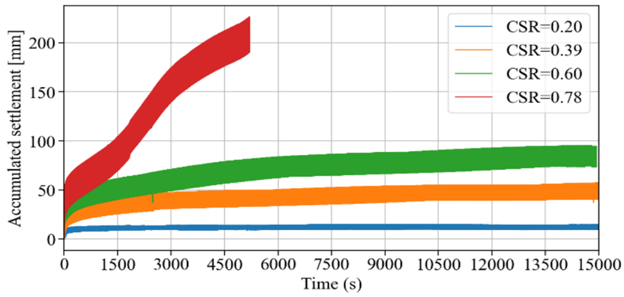

Fig 12. Accumulated settlement versus time.

Fig. 12 shows the development of accumulated settlement with time under different CSR values. As the CSR increased, the accumulated settlement increased progressively. When CSR = 0.20, 0.39, and 0.60, settlement increased rapidly during the first few loading cycles, after which the rate of settlement accumulation gradually decreased with increasing number of cycles and eventually approached a relatively stable level. In contrast, when CSR = 0.78, settlement continued to develop rapidly throughout the test, reaching 100 mm at nearly 2000 cycles and exceeding 200 mm after 4500 cycles, indicating clear failure.

6 Conclusion

This paper presents a testing system capable of applying controlled cyclic loading to a circular loading plate on

peat, together with some preliminary test results. The main conclusions are as follows:
1. The double-hinged actuator configuration, combined with an appropriately designed reaction frame, made it possible to apply controlled cyclic loading to a circular loading plate on peat, providing a reliable test method for investigating the in situ response of peat under cyclic loading.
2. Owing to the heterogeneity of peat, fluctuations were observed in the CPT q_{net} profiles. However, the relative difference in the median q_{net} values within the peat layer remained within 30%, indicating good repeatability among the different loading tests.
3. The static loading test on the non-preloaded peat gave a bearing capacity of 68 kPa. Based on this value, different cyclic stress ratios were defined for the cyclic loading tests. When CSR was lower than 0.60, the settlement rate gradually decreased, and the accumulated settlement tended to stabilise. In contrast, when CSR was 0.78, settlement continued to develop until failure occurred.
4. The test results will provide valuable validation data for advanced numerical techniques and predictive models for peat under cyclic loading.

The authors acknowledge the ProRail and research program RESET for financing the system design and field tests. The authors would also like to express their sincere gratitude to Jens van den Berg and Jaap Elstgeest for their assistance and advice regarding actuator configuration, assembly design, and field work.

References

1. G. Kruse, E. Den Haan, Characterisation and engineering properties of dutch peats, in Second International Workshop on Characterisation and Engineering Properties of Natural Soils (2006), 2101-2133.
2. E. Den Haan, A. Feddema, Deformation and strength of embankments on soft dutch soil. Proc. Inst. Civ. Eng. Geotech. Eng. **166**, 239–252 (2013). https://doi.org/10.1680/geng.9.00086
3. S. Muraro, C. Jommi, Experimental determination of the shear strength of peat from standard undrained triaxial tests: correcting for the effects of end restraint. Géotechnique **71**, 76–87 (2021). https://doi.org/10.1680/jgeot.18.P.346
4. A. Lemnitzer, R. Cappa, S. Yniesta, S. Brandenberg, Centrifuge testing of model levees atop peat: experimental data. Earthquake Spectra **32**, 1903–1924 (2016). https://doi.org/10.1193/032715EQS048
5. M. Long, Centrifuge modelling of sand and sawdust embankments on peat for sustainable infrastructure development, in Proceedings of the XVIII ECSMGE 2024 (2024)
6. C. Zwanenburg, G. Erkens, Uitdam, the Netherlands: test site for soft fibrous peat. AIMS Geosci. **5**, 804–830 (2019). https://doi.org/10.3934/geosci.2019.4.804
7. C. Chen, Z. Zhou, X. Zhang, G. Xu, Behavior of amorphous peaty soil under long-term cyclic loading. Int. J. Geomech. **18**, 04018115 (2018). https://doi.org/10.1061/(ASCE)GM.1943-5622.0001254
8. J. Tong, T. Wu, L. Guo, Z. Yuan, H. Jin, Long-term cyclic behavior of soft clay under different variable confining pressures and partially drained conditions. Transp. Geotech. **33**, 100723 (2022). https://doi.org/10.1016/j.trgeo.2022.100723
9. C. Chen, G. Xu, Z. Zhou, L. Kong, X. Zhang, S. Yin, Undrained dynamic behaviour of peaty organic soil under long-term cyclic loading, part II: constitutive model and simulation. Soil Dyn. Earthquake Eng. **129**, 105902 (2020). https://doi.org/10.1016/j.soildyn.2019.01.039
10. C. Zwanenburg, R. J. Jardine, Laboratory, in situ and full-scale load tests to assess flood embankment stability on peat. Géotechnique **65**, 309–326 (2015). https://doi.org/10.1680/geot.14.P.257
11. R. J. Jardine, Geotechnics, energy and climate change: the 56th rankine lecture. Géotechnique **70**, 3–59 (2020). https://doi.org/10.1680/jgeot.18.RL.001
12. H. T. L. Massop, Monitoring long-term peat subsidence with subsidence platens in zegveld, the Netherlands. Geoderma **450**, 1–16 (2024). https://doi.org/10.1016/j.geoderma.2024.117039
13. C. Zwanenburg, M. Konstadinou, E. Grünewald, Geotechnical characterization and strain-rate dependent response of peat from the Netherlands. AIMS Geosci. **11**, 923–945 (2025). https://doi.org/10.3934/geosci.2025040
14. J. Zhang, T. De Gast, C. Zwanenburg, K. Gavin, Full-scale load tests to assess the bearing capacity of peat at zegveld. AIMS Geosci. **11**, 828–845 (2025). https://doi.org/10.3934/geosci.2025035
15. B. Z. Coelho, J. Priest, P. Hölscher, Dynamic behaviour of transition zones in soft soils during regular train traffic. Proc. Inst. Mech. Eng. F: J. Rail Rapid Transit **232**, 645–662 (2018). https://doi.org/10.1177/0954409716683078
16. J. Liu, J. Xiao, Experimental study on the stability of railroad silt subgrade with increasing train speed. J. Geotech. Geoenviron. Eng. **136**, 833–841 (2010). https://doi.org/10.1061/(ASCE)GT.1943-5606.0000282
17. M. Singh, B. Indraratna, T. T. Nguyen, Experimental insights into the stiffness degradation of subgrade soils prone to mud pumping. Transp. Geotech. **27**, 100490 (2021). https://doi.org/10.1016/j.trgeo.2020.100490
18. Deltares, Analysis of actual axle loads, related to embankment stability, 11207168-010-GEO-0001 (2022)
19. Deltares, Three-dimensional dynamic finite element analysis of embankments, 11207168-011-GEO-0001 (2022)
20. Y. Cai, L. Xu, W. Liu, Y. Shang, N. Su, D. Feng, Field test study on the dynamic response of the cement-improved expansive soil subgrade of a heavy-haul railway. Soil Dyn. Earthquake Eng. **128**, 105878 (2020). https://doi.org/10.1016/j.soildyn.2019.105878
21. B. Indraratna, T. Ngo, F. B. Ferreira, C. Rujikiatkamjorn, A. Tucho, Large-scale testing facility for heavy haul track. Transp. Geotech. **28**, 100517 (2021). https://doi.org/10.1016/j.trgeo.2021.100517
22. T. Lunne, P. K. Robertson, J. J. M. Powell, Cone penetration testing in geotechnical practice (CRC Press, London, 1997)